ACS APPLIED MATERIALS & INTERFACES

Research Article

www.acsami.org

Robust Polyaniline–Graphene Complex Counter Electrodes For Efficient Dye-Sensitized Solar Cells

Benlin He, Qunwei Tang,* Min Wang, Haiyan Chen, and Shuangshuang Yuan

Institute of Materials Science and Engineering, Ocean University of China, Qingdao 266100, P.R. China

ABSTRACT: With an aim of accelerating the charge transfer between polyaniline (PANi) and graphene, polyaniline–graphene (PANi–graphene) complexes are synthesized by a reflux technique and employed as counter electrodes (CEs) for dye–sensitized solar cells (DSSCs). Because of the easy charge-transfer between PANi (*N* atoms) and graphene (*C* atoms) by a covalent bond, electrical conduction and electrocatalysis of PANi-graphene complex CEs, and therefore power conversion efficiency of their DSSCs have been elevated in comparison with that of PANi–only CE. The resultant PANi–graphene complex CEs are characterized by spectral analysis, morphology observation, and electrochemical tests. The DSSC employing PANi–8 wt ‰ graphene complex CE gives an impressive power conversion efficiency of 7.78%, which is higher than 6.24% from PANi–only and 6.52% from Pt–only CE–based DSSCs.

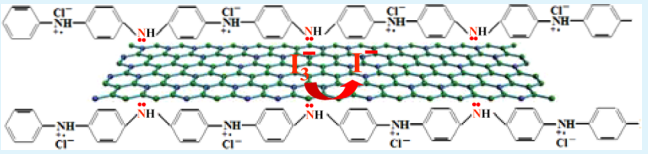

KEYWORDS: *counter electrode, polyaniline–graphene complex, charge transfer, dye–sensitized solar cells*

INTRODUCTION

Dye–sensitized solar cells (DSSCs) have attracted intensive attention because of their merits on low fabrication cost, relatively high power conversion efficiency, and environmental friendliness.[1] A typical DSSC device comprises a dye–sensitized TiO_2 photoanode, redox electrolyte, and a counter electrode (CE). The CE is a crucial component for achieving high photovoltaic performances for a DSSC device. Pt–related materials often serve as CEs because of good electron–conducting ability and high electrochemical activity toward triiodide reduction, however, Pt is relatively expensive because of its scarce resource in the earth.[2] Therefore, it is highly desirable to develop competent substitutes in order to reduce the overall fabrication cost with no sacrifice of photovoltaic performances of DSSCs. Conducting polymers, such as polyaniline (PANi),[3,4] polypyrrole,[5,6] and poly(3,4–ethylenedioxythiophene) (PEDOT),[7,8] are promising alternative materials in CEs. Among them, PANi has been considered as one of the most preferred CE material owing to its easy fabrication, low cost, high electrochemical activity, and environmental stability. However, the electric-conducting ability of PANi is relatively low in comparison with Pt–based materials, which may cause photocurrent loss in the cell circuit and further drag on photovoltaic performances.

Except for PANi, graphene (a single–layer material of sp^2–bonded carbon atoms in a hexagonal lattice) has an excellent electrical conduction in two dimensions, high strength, and surface area.[9,10] However, one of the drawbacks of graphene is its unsatisfactory redox behaviors. A compromise approach of fabricating efficient CE materials is to integrate the rapid charge transfer ability of graphene with good redox performance of PANi.[11,12] However, low solubility of pristine graphene in most organic solvents has been the main barrier for their chemical manipulation, quantitative characterization and potential use. Many efforts have been made to overcome this disadvantage, a routine approach is the *in–situ* polymerization of aniline monomers in graphene oxide and obtain reduced PANi/graphene through a reduction step.[11] Although the use of graphene oxide can improve the dispersion of reduced graphene in polymers, they always suffer from chemical reduction which is not easy to control O/C ratio and can destroy the well-defined conjugated alignment. The oxidation is expected to weaken the physical, chemical, and electrochemical properties of graphene. Moreover, PANi/graphene composites can also be directly prepared by chemical, physical or electrochemical codeposition method, giving an insurmountable weakness for CE applications: The physical combination of PANi and graphene results in a relatively high interfacial resistance and therefore low charge-transfer kinetics between them. In other words, graphene does not fulfill its good charge–transfer function and transfer returned electrons (the electrons from external circuit to CE) to PANi for participating reduction reaction of triiodides. Therefore, the power conversion efficiencies of the resultant DSSCs based on PANi/graphene CEs are still not satisfactory.

In the search for more robust PANi-graphene composite CEs, here we pioneerly report that aniline monomers can be employed to functionalize and solubilize graphene by forming donor–acceptor complexes during a reflux process. As shown in Figure 1, there are covalent bonds between aniline (N atoms) and graphene (C atoms) in the resultant aniline–graphene complex, therefore, the returned electrons can be easily transferred from graphene to PANi by covalent bonds. The structure, morphology, and electrochemical performances of the PANi–graphene complex CEs are characterized. Results reveal that the PANi–graphene complexes can enhance photovoltaic

Received: February 16, 2014
Accepted: May 14, 2014
Published: May 14, 2014

   dx.doi.org/10.1021/am500981w | *ACS Appl. Mater. Interfaces* 2014, 6, 8230–8236

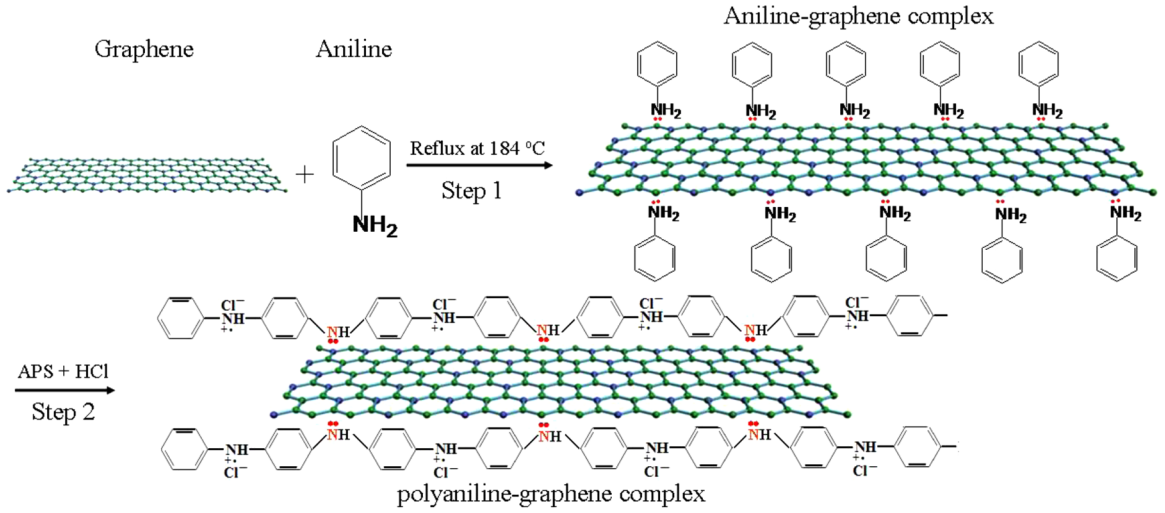

Figure 1. Synthesis route and proposed complexation mechanism between PANi and graphene by a reflux procedure.

performances of DSSCs because of their improved charge−transfer kinetics.

EXPERIMENTAL SECTION

Reflux Synthesis of Aniline−Graphene Complexes. The aniline−graphene complexes were synthesized by a reflux process. In details, five aniline−graphene mixtures at graphene dosages of 1, 4, 8, 10, and 15 wt ‰ were sealed in a three−neck flask filled with high−purity N_2 gas. The mixtures were refluxed in dark for 6 h at 184 °C to obtain the target aniline−graphene complexes, which were subsequently stored in a dark and cold atmosphere.

Fabrication of PANi−Graphene Complex CEs. Fifty milliliters of aqueous solution consisting of HCl (1 M) and $(NH_4)_2S_2O_8$ (APS) was dipped into 50 ml of a mixture consisting of HCl (1 M) and aniline-graphene complex (0.325 M) at 0 °C within 2 h. Before polymerization reaction, pretreated fluorine−doped tin oxide (FTO, sheet resistance was 12 Ω sq^{-1}) glass substrate was horizontally put at the bottom of a container. After reaction at 4 °C for 10 h, the FTO glass substrate was successively rinsed with 1 M HCl aqueous solution and deionized water to remove unreacted aniline monomers and oligomers. Finally, the FTO supported PANi−graphene complex CEs were vacuumly desiccated at 50 °C for 24 h. As a comparison, PANi−only CE was also prepared under the same conditions.

Assembly of DSSCs. A layer of TiO_2 nanocrystal anode film with a thickness of 10 μm was prepared by a sol−hydrothermal method. After air drying, the colloid was calcined at 450 °C for 30 min to obtain TiO_2 nanocrystal anode film which were subsequently immersed into a 0.5 mM ethanol solution of N719 dye ([*cis*-di(thiocyanato)-*N*,*N*′-bis(2,2′-bipyridyl-4-carboxylic acid)-4-tetrabutylammonium carboxylate], purchased from Dyesol LTD, Australia). The DSSC with an active area of 0.25 cm^2 was fabricated by combining a dye-sensitized TiO_2 anode and an FTO supported PANi-graphene complex CEs. A redox electrolyte consisted of 100 mM tetraethylammonium iodide, 100 mM tetramethylammonium iodide, 100 mM tetrabutylammonium iodide, 100 mM NaI, 100 mM KI, 100 mM LiI, 50 mM I_2, and 500 mM 4-*tert*-butyl-pyridine in 50 mL of acetonitrile.

Electrochemical Characterizations. The electrochemical performances were recorded on a conventional three−electrode cell comprising an Ag/AgCl reference electrode, a CE of platinum sheet, and a working electrode of FTO glass supported PANi−graphene complex. The cyclic voltammetry (CV) curves were recorded from −0.5 to +1.6 V and back to −0.5 V. Before the measurement, the supporting electrolyte consisting of 50 mM LiI, 10 mM I_2, and 500 mM $LiClO_4$ in acetonitrile was degassed using nitrogen for 10 min. Electrochemical impedance spectroscopy (EIS) measurements were also carried out on the CHI660E electrochemical workstation (CHI660E, Shanghai Chenhua Device Company, China) in a frequency range of 0.01 Hz ~ 10^5 kHz and an ac amplitude of 10 mV at room temperature. The resultant impedance spectra were analyzed using the Z−view software. Tafel polarization curves were recorded on the same workstation by assembling symmetric cell consisting of FTO−PANi−graphene complexlelectrolytelFTO−PANi−graphene complex. The curves were recorded by scanning potential window of −1 to 1 V at a scan rate of 10 mV s^{-1}.

Photovoltaic Tests. The photovoltaic tests of the DSSC were carried out by measuring the current-voltage (J−V) characteristic curves using an electrochemical workstation under irradiation of a simulated solar light from a 100 W Xenon arc lamp (XQ−500 W) in ambient atmosphere. The incident light intensity was controlled at 100 mW cm^{-2} (AM1.5) which was calibrated using a FZ−A type radiometer from Beijing Normal University Photoelectric Instrument Factory. Each DSSC device was measured five times to eliminate experimental error and a compromise J−V curve was employed.

Other Characterizations. The morphologies of the resultant PANi or PANi−graphene complex CEs were observed with a scanning electron microscope (SEM, S4800). Fourier transform infrared spectrometry (FTIR) spectra were recorded on a PerkinElmer spectrum 1760 FTIR spectrometer. The UV−vis spectra were measured on a UV−3200 spectrophotometer by dissolving the samples in deionized water. The fluorescence emission spectra were recorded at room temperature using a Fluorolog3−P spectrophotometer. The emission spectrum was collected using a conventional setup at excitation wavelengths of 500 nm.

RESULTS AND DISCUSSION

To reveal the complexing mechanism of aniline monomers onto graphene, UV−vis adsorption spectra of graphene, aniline, aniline−8 wt ‰ graphene mixture, and aniline−graphene complexes with various graphene dosages are diluted in acetone. As is shown in Figure 2, no peak is observed in the UV−vis spectrum ranging from 350 to 700 nm. In comparison with the UV−vis spectrum of aniline−graphene mixture, new absorption peaks at 366, 458, 513, and 552 nm are detected in aniline−graphene complexes, suggesting that aniline-graphene complexes have been successfully formed during the reflux process.[13,14] At elevated temperature, such as 184 °C, graphene and aniline are believed to form a charge−transfer complex in its ground state because graphene is a good electron acceptor, whereas aniline is a fairly good electron donor, as evidenced by the appearance of the new absorptions.

The polymerization of conjugated PANi suffers from dimers, trimers, oligomers and polymer in the presence of APS and protonic acid.[15] As shown in Figure 1, each imine group (−NH−) has a pair of lone-electrons which can share with a

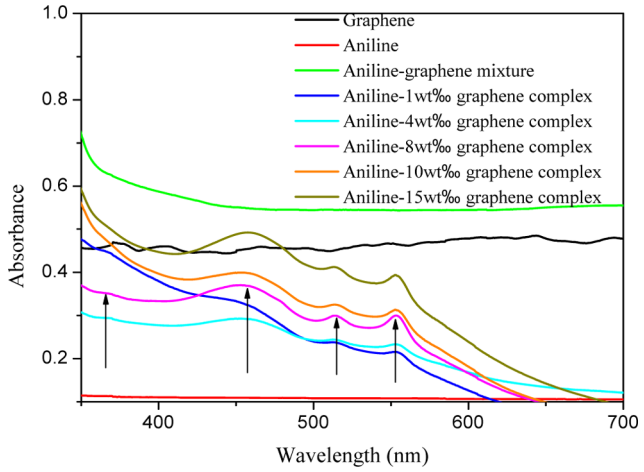

Figure 2. UV−vis absorption spectra of graphene, aniline, aniline−8 wt % graphene mixture, and aniline−graphene complexes diluted in acetone at graphene dosages of 1, 4, 8, 10, and 15 wt ‰.

carbon atom in conjugation structure of graphene (−C═) to form a covalent bond. There is a consensus that the chemical bonding between PANi and graphene can accelerate the charge-transfer.[16−18] Furthermore, previous research also validates that the resultant PANi chains are intertwisted to form agglomerated nanoparticles in traditional chemical polymerization because of the strong intramolecular and intermolecular hydrogen bonding,[19,20] resulting in low electron delocalization, short−range charge−transfer, and therefore poor electrical and electrochemical performances. The parallel bonding can enhance the well−aligned arrangement of PANi chains along the surface of graphene, which is expected to give extraordinary synergistic effect in accelerating charge transfer along PANi chains.

A prerequisite of fabricating robust PANi−graphene complexes with rapid charge−transfer is the successful attachment of aniline onto graphene. Figure 3a gives fluorescence emission spectra of graphene, pure aniline, and resultant aniline−graphene complexes diluted with acetone solvent. The maximum emissions in acetone are at around 575 and 620 nm, whereas the fluorescence spectra of graphene and pure aniline are generally quenched. The fluorescence excitation spectra of the aniline−graphene complexes are quite different from the absorption spectra of the individual components, indicating the formation of a new light−absorbing species. It is noteworthy to mention that the red shift of maximum emission, as is shown in Figure 3b−f, is in an order of acetone, toluene, and methanol, which are believed to be the major contributions of their polarities to $\pi-\pi$ stacking resulted from the electrostatic interactions and hydrophobic effects.[21]

Figure 4 displays the FTIR spectra of PANi and PANi−graphene complexes at various graphene dosages. The main absorption bands situated at ca. 795, 1093, 1296, 1480, and 1560 cm^{-1} are attributed to the following vibration modes: bending of C−H (out-of-plane) on benzene ring (B), bending of C−H (in-plane), mode of N═quinoid ring (Q)═N, stretching of aromatic-N, stretching of N−B−N, and stretching of N═Q═N.[22,23] In comparison with PANi, the FTIR spectra of PANi-graphene complexes determine the appearance of the 1034 cm^{-1} band, especially at a high graphene dosage. The appearance of this vibration absorption band indicates a charge-transfer and a selective interaction of the graphene fragments with quinoid rings of PANi backbones.[24] A similar interaction between carbon nanotubes and PANi quinoid rings has also been detected in PANi/multiwalled carbon nanotubes.[25]

The microstructure of the bared PANi coated FTO electrode is observed by SEM, as shown in Figure 5a, suggesting that the PANi are composed of compact aggregations because of strong intramolecular and intermolecular hydrogen-bonding. This closely packed structure provides increased interfacial resistance for charger transfer and penetration resistance for exchange of I^-/I_3^- redox couples. It is expected that PANi−8 wt ‰ graphene complex CE has a looser and porous structure, as shown in Figure 5b. The homogeneous nanostructures suggest that PANi molecular chains have been parallelly attached on graphene surface by covalent bonds. The morphological observation further validates the rationality of the proposed complexation mechanism in Figure 1. The porous structure is expected to enhance the electrolyte loading and to facilitate the migration of I^-/I_3^- redox couples within PANi−graphene complex CEs.

CV is an efficient tool for analyzing the electrocatalytic activities of CEs toward I^-/I_3^- redox species. The CV curves of the resultant complex CEs in liquid electrolyte were recorded. As a reference, PANi−only CE was also performed at the same conditions. As is shown in Figure 6, the peak positions and shapes of the CV curves from PANi−graphene complex CEs are very similar to those of Pt and PANi−only CE, revealing that PANi−graphene complex CEs have a similar electrocatalytic activity to Pt CE. Considering that the task of CE is to reduce I^-/I_3^- redox species, mediators in regenerating the sensitizer after electron injection in a liquid−state DSSC, the electro-reduction reaction of $I_3^- + 2e \rightarrow 3I^-$ can be employed to elevate the electrocatalytic activity of PANi−graphene complex CEs (see the inset). Notably, the combination of graphene with PANi increases the peak current density and decreases the peak−to−peak separation. The higher peak current densities and lower peak−to−peak separation suggest an enhanced electroreductive behavior to I^-/I_3^- redox couples. It is noteworthy to mention that the PANi−8 wt ‰ graphene complex CE has the highest electrocatalytic activity toward triiodide reduction. The increase in the number of bonding sites between PANi and graphene in graphene dosage of 1−8 wt ‰ has a promotion effect on electrocatalytic performance of PANi-graphene complex CE. However, the resultant PANi-graphene complexes have less bonding sites because of aggregations of disordered graphene, which results in a low charge−transfer kinetics between PANi and graphene.

From the stacking CV curves of PANi−8 wt ‰ graphene complex CE at different scan rates, one can find an outward extension of all the redox peaks (Figure 7a). Linear relationships are observed by plotting peak current density corresponding to $I_3^- \leftrightarrow I^-$ versus square root of scan rate, as shown in Figure 7b. This result indicates the redox reaction of iodides within PANi−8 wt ‰ graphene complex CE is controlled by ionic diffusion in the electrolyte, and the transfer rate of both electrons and ions are fast enough for the reduction rate of triiodides on the surface of PANi−8 wt ‰ graphene complex CE. This result also suggests that the adsorption of iodide species is hardly affected by the redox reaction on the PANi−8 wt ‰ graphene complex CE surface and no specific interaction occurred between I^-/ I_3^- and the CE.[26]

With an aim of further elucidating the catalytic activities of PANi−graphene complex CEs toward the reduction reaction of $I_3^- \rightarrow I^-$, EIS experiments were carried out in a symmetric cell fabricated by two identical CEs. Nyquist plots in Figure 8 illustrate impedence characteristics of PANi−only and PANi−graphene complex CEs. According to the equivalent circuit (inset of Figure 8), the intercept on the real axis represents the series resistance (R_s). The arc arises from the charge−transfer resistance (R_{ct}) at CE/electrolyte interface, which changes inversely

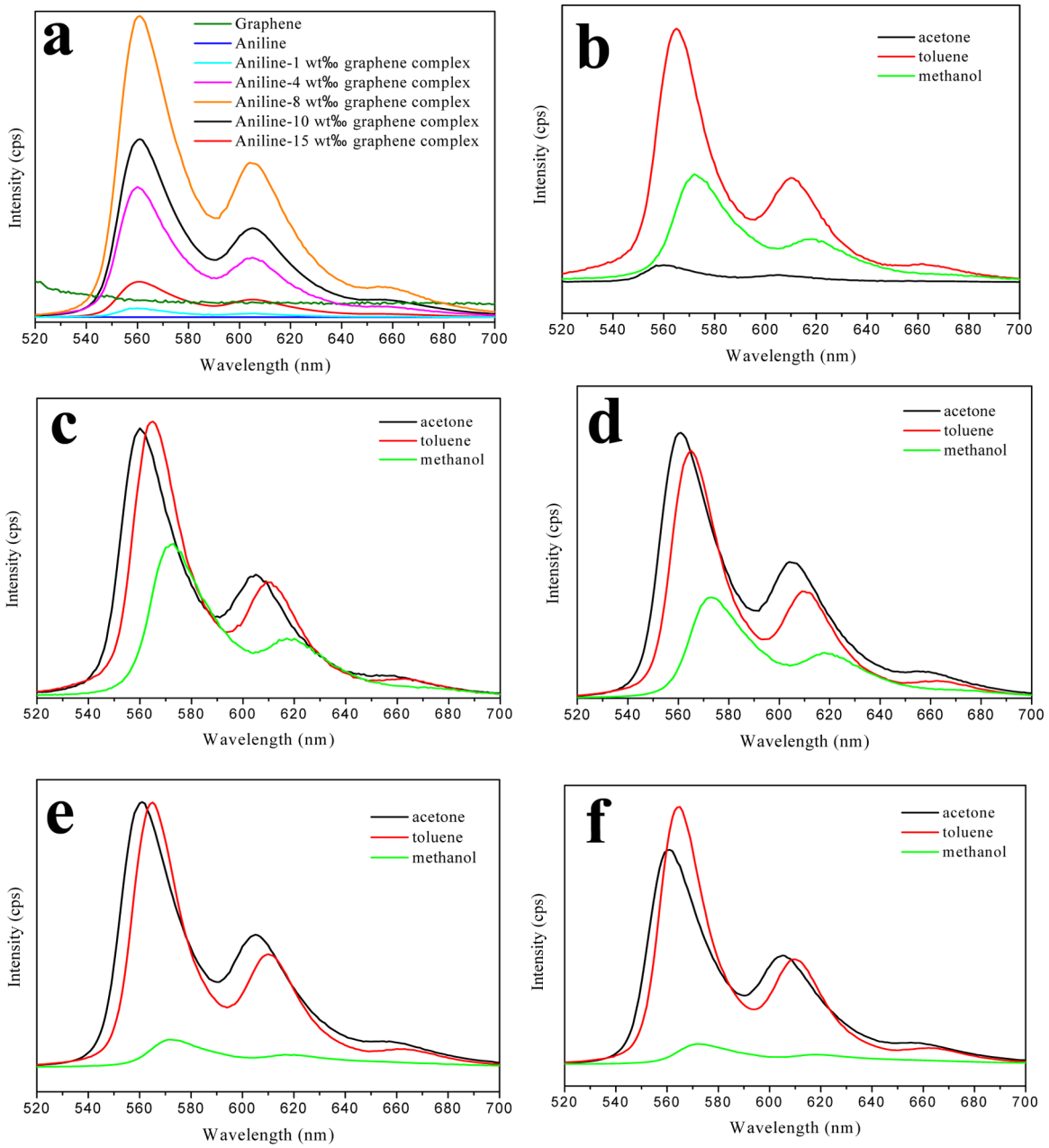

Figure 3. (a) Emission spectra of graphene, aniline, and aniline−graphene complexes in acetone at graphene dosages of 1, 4, 8, 10, and 15 wt ‰. Emission spectra of aniline−graphene complexes at graphene dosages of (b) 1, (c) 4, (d) 8, (e) 10, and (f) 15 wt ‰ diluted in organic solvents: acetone, toluene, and methanol. The excitation wavelength was 500 nm. All the solutions were in their saturation states.

with the electrocatalytic activity of CEs on the reduction of triiodide, whereas W represents the Nernst diffusion impedance corresponding to the diffusion resistance of I^-/I_3^- redox species. Constant phase element (CPE) is frequently used as a substitute for a capacitor in an equivalent circuit to fit the impedance behavior of the electrical double layer. These electrochemical parameters were obtained by fitting EIS spectra using a Z−view software and summarized in Table 1. There is a good agreement between measured and fitted curves. The PANi-8 wt ‰ graphene complex CE has the smallest R_{ct}, indicating the highest electrocatalytic activity toward triiodide reduction. Moreover, the order of W, diffusion resistance of I^-/I_3^-, against graphene dosage is the same to that of R_{ct}. For the complex CEs at high graphene dosages, the increased number in covalent bonds can accelerate the electron transfer from graphene to PANi and participate in the reduction reaction of triiodides, once the triiodides are reduced to iodides, they will diffuse to anode/electrolyte interface for dye recovery. Therefore, the enhancement in electrocatalytic performance by increasing graphene dosage has an acceleration effect on the diffusion of redox species. The conclusions for the electrocatalytic activity and diffusion derived from EIS and CV data are consistent.

Tafel polarization curves were recorded to further reveal the interfacial charge-transfer properties at the CE/electrolyte interface, as presented in Figure 9. The larger slope for the anodic or cathodic branch indicates a higher exchange current density (J_0) on the electrode and better catalytic activity toward triiodide reduction. Apparently, the obtained J_0 from PANi−graphene complex CEs are larger than that of Pt−only or PANi−only CE, indicating that the charge−transfer ability has been

dx.doi.org/10.1021/am500981w | ACS Appl. Mater. Interfaces 2014, 6, 8230−8236

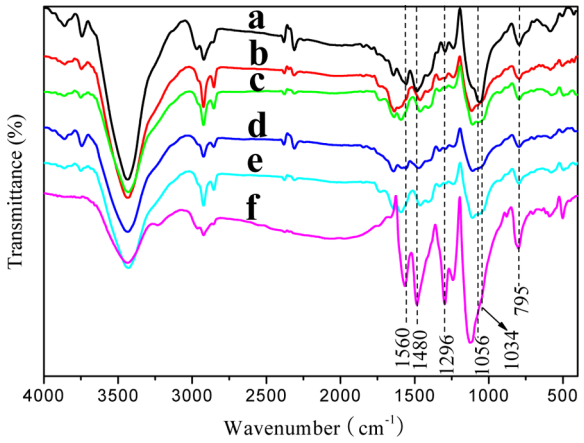

Figure 4. FTIR spectra of (a) PANi and PANi–graphene complexes at graphene dosages of (b) 1, (c) 4, (d) 8, (e) 10, and (f) 15 wt ‰.

Table 1. Parameters for Equivalent Circuit Obtained by Fitting EIS Data Using a Z–View Software

CEs	R_s (Ω cm^2)	R_{ct} (Ω cm^2)	CPE-T	CPE-P	W (Ω cm^2)
PANi	147.40	188.80	7.78×10^{-4}	0.72	8.90
PANi–1 wt ‰ graphene complex	6.03	48.24	2.65×10^{-3}	0.71	5.24
PANi–4 wt ‰ graphene complex	6.81	14.64	3.30×10^{-3}	0.81	0.81
PANi–8 wt ‰ graphene complex	7.64	4.96	8.41×10^{-3}	0.74	0.66
PANi–10 wt ‰ graphene complex	8.74	79.54	1.35×10^{-3}	0.72	28.93
PANi–15 wt ‰ graphene complex	3.12	142.20	2.54×10^{-3}	0.74	29.22
Pt	23.40	13.00	1.29×10^{-5}	0.94	1.75

enhanced by fabricating complexes. In comparison with PANi–only CE, the enhanced J_0 from PANi–graphene complex derives from the porous structure and easy charge–transfer, as shown in SEM image and proposed mechanism.[27] The intersection of the cathodic branch with the Y–axis can be considered as the limiting diffusion current density (J_{lim}), depending on the diffusion coefficient of I^-/I_3^- couples in electrolyte, which determined by the diffusion properties of the redox couple and the CE catalysts.[28] The diffusion coefficient (D_n) of redox couples is in linear with J_{lim} according to eq 1[29]

$$D_n = lJ_{lim}/2nFC \quad (1)$$

where l is the spacer thickness and C is the concentration of triiodide ions. From the stacking tafel curves, it is apparently that most of the

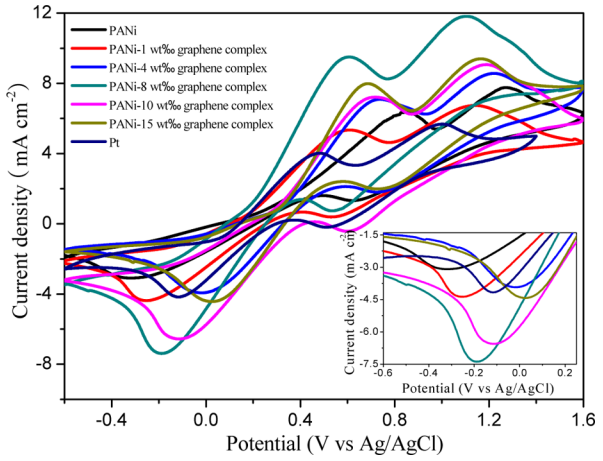

Figure 6. CV curves of Pt, PANi, and PANi-graphene complex CEs for I^-/I_3^- redox species recorded at a scan rate of 50 mV s^{-1}. The inset is the figure on magnified CV curves for the first reduction peak in a potential scale of −0.6–0.25 V.

Table 2. Comparison of Short–Circuit Current Density (J_{sc}), Open–Circuit Voltage (V_{oc}), Fill Factor (FF), and Power Conversion Efficiency (η) in the Resultant DSSCs

	photovoltaic parameters			
CEs	J_{sc} (mA cm^{-2})	V_{oc} (V)	FF	η (%)
PANi	11.96	0.712	0.73	6.24
PANi–1 wt ‰ graphene complex	13.84	0.726	0.67	6.71
PANi–4 wt ‰ graphene complex	15.68	0.696	0.64	7.03
PANi–8 wt ‰ graphene complex	14.85	0.737	0.71	7.78
PANi–10 wt ‰ graphene complex	16.33	0.705	0.63	7.24
PANi–15 wt ‰ graphene complex	14.97	0.712	0.65	6.89
Pt	13.93	0.714	0.66	6.52

PANi–graphene complex CEs have larger J_{lim} than that of pure Pt and PANi CEs. The results suggest enhanced diffusion kinetics for I^-/I_3^- redox species in liquid electrolyte by employing PANi-graphene complex CEs. And the PANi–8 wt ‰ graphene complex CE shows the highest D_n, which is consistent with CV and EIS ananlysis.

Figure 10 shows the photovoltaic characteristics of DSSCs from pure PANi and PANi–graphene complex CEs and the parameters reflecting DSSC properties are summarized in Table 2. The DSSCs employing PANi-graphene complex CEs achieve higher J_{sc} than that fabricated using a PANi–only CE. This might be attributed to the good dispersion of PANi–graphene complexes, which provides larger active surface areas for triiodides

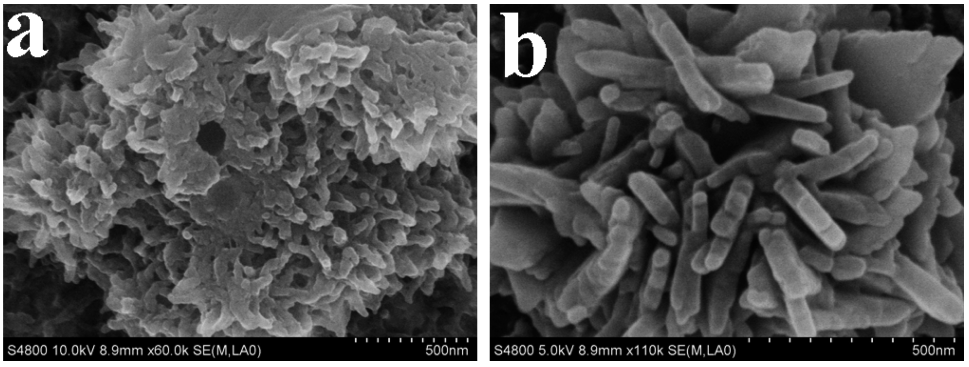

Figure 5. SEM photographs of (a) PANi and (b) PANi–8 wt ‰ graphene complex CEs.

dx.doi.org/10.1021/am500981w | ACS Appl. Mater. Interfaces 2014, 6, 8230–8236

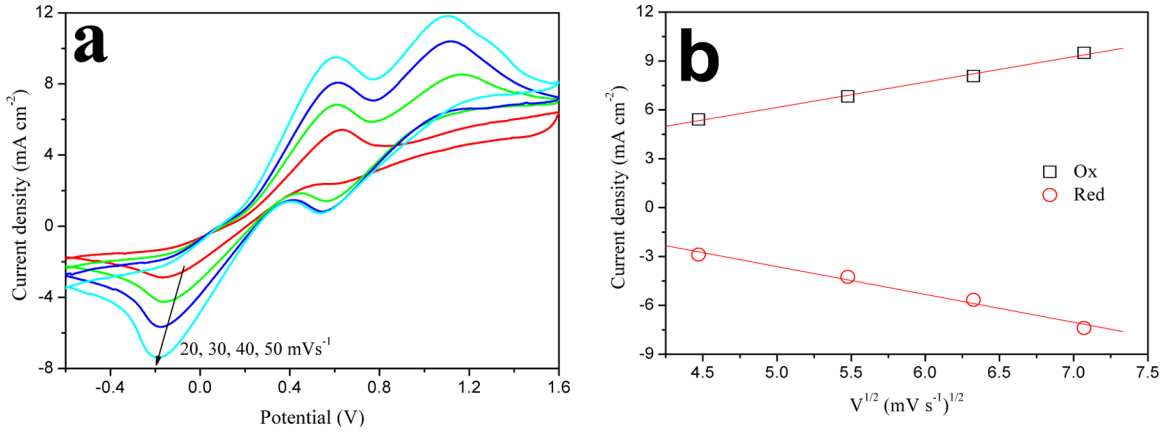

Figure 7. (a) CV curves of PANi-8 wt ‰ graphene complex CE for I^-/I_3^- redox species at varied scan rates, and (b) relationship between peak current density and square root of scan rate.

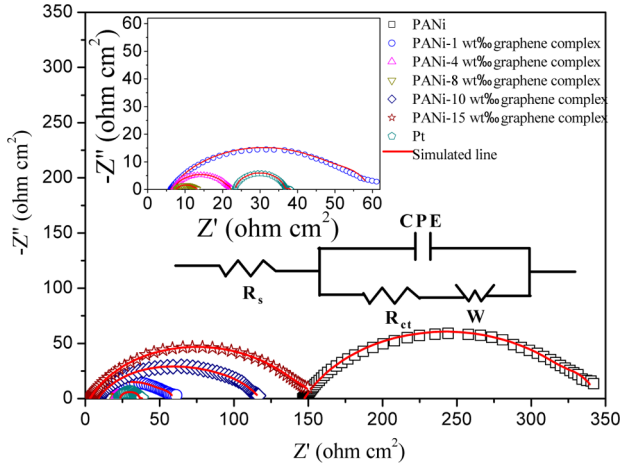

Figure 8. Nyquist plots for symmetric cells fabricated with identical Pt, PANi–only, and PANi–graphene complex CEs. The lines express fit results for corresponding EIS data, and the insets give an equivalent circuit and magnified EIS plots.

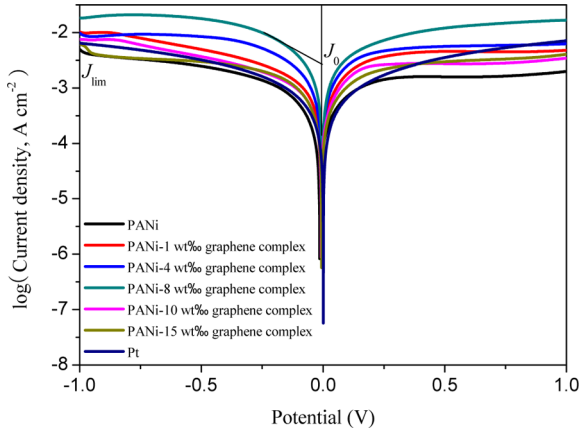

Figure 9. Tafel polarization curves of symmetrical cells fabricated with identical Pt, PANi–only, and PANi–graphene complex CEs that are same as the ones used in EIS experiments.

reduction. The PANi–graphene complex, prepared at the optimal condition in this study, improves the charge–transfer ability within CEs, which is evident in the higher J_{sc} observed for the DSSCs. There is a significant enhancement in η of the resultant DSSC, and the highest η is 7.78% in PANi–8 wt ‰ graphene complex CE

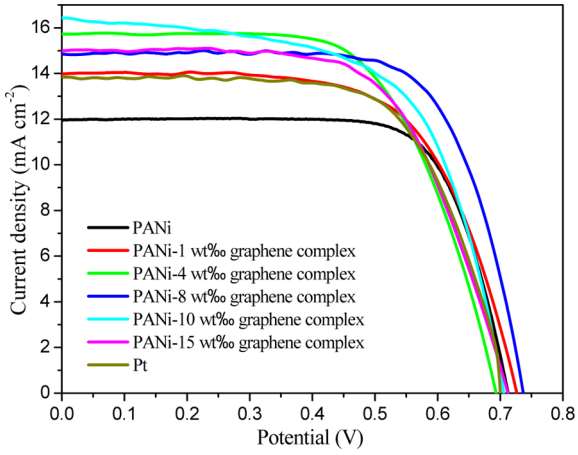

Figure 10. *J*–*V* characteristics of DSSCs from pure PANi and PANi–graphene complex CEs.

based DSSC in comparison with that of 6.24% from PANi–only CE and 6.52% from pure Pt CE. After performing a comprehensive analysis of the DSSCs, it can be concluded that the photovoltaic performance is in agreement with the EIS and Tafel polarization results.

CONCLUSIONS

In conclusion, we have demonstrated that fabrication of PANi–graphene complex CEs by a reflux technique is an effective strategy for accelerating the charge transfer with the complexes. New light–absorbing species and absorption bands can be detected from the fluorescence excitation and UV–vis absorption spectra of aniline-graphene complexes. Covalent bonds between PANi (–NH–) and graphene (–C═) are expected to accelerate the charge transfer. The DSSC from PANi–8 wt ‰ graphene complex CE provides an impressive power conversion efficiency of 7.78% in comparison with that of 6.24% from pure PANi CE and 6.52% from Pt CE. The research presented here is far from being optimized but these profound advantages along with low–cost synthesis and scalable materials promise the new PANi–graphene complex CEs to be strong candidates in robust DSSCs.

AUTHOR INFORMATION

Corresponding Author

*E-mail: tangqunwei@ouc.edu.cn. Tel/Fax: 86-532-66781690.

Notes

The authors declare no competing financial interest.

■ ACKNOWLEDGMENTS

The authors gratefully acknowledge Ocean University of China for providing Seed Fund to this project, and Fundamental Research Funds for the Central Universities (201313001, 201312005), Shandong Province Outstanding Youth Scientist Foundation Plan (BS2013CL015), Doctoral Fund of Ministry of Education of China (20130132120023), Shandong Provincial Natural Science Foundation (ZR2011BQ017), and Research Project for the Application Foundation in Qingdao (13-1-4-198-jch).

■ REFERENCES

(1) Chung, I.; Lee, B.; He, J.; Chang, R. P. H.; Kanatzidis, M. G. All-Solid-State Dye-Sensitized Solar Cells with High Efficiency. *Nature* **2012**, *485*, 486−489.

(2) Olsen, E.; Hagen, G.; Linquist, S. E. Dissolution of Platinum in Methoxy Propionitrile Containing LiI/I_2. *Sol. Energy Mater. Sol. C* **2000**, *63*, 267−273.

(3) Li, Q. H.; Wu, J. H.; Tang, Q. W.; Lan, Z.; Li, P. J.; Lin, J. M.; Fan, L. Q. Application of Microporous Polyaniline Counter Electrode for Dye-Sensitized Solar Cells. *Electrochem. Commun.* **2008**, *10*, 1299−1302.

(4) Wang, H.; Feng, Q.; Gong, F.; Li, Y.; Zhou, G.; Wang, Z. S. In Situ Growth of Oriented Polyaniline Nanowires Array for Efficient Cathode of Co(III)/Co(II) Mediated Dye-Sensitized Solar Cell. *J. Mater. Chem. A* **2013**, *1*, 97−104.

(5) Jeon, S. S.; Kim, C.; Ko, J.; Im, S. S. Spherical Polypyrrole Nanoparticles As a Highly Efficient Counter Electrode for Dye-Sensitized Solar Cells. *J. Mater. Chem.* **2011**, *21*, 8146−8151.

(6) Bu, C.; Tai, Q.; Liu, Y.; Guo, S.; Zhao, X. A Transparent and Stable Polypyrrole Counter Electrode for Dye-Sensitized Solar Cell. *J. Power Sources* **2013**, *221*, 78−83.

(7) Xiao, Y. M.; Lin, J. Y.; Wu, J. H.; Tai, S. Y.; Yue, G. T. Pulse Potentiostatic Electropolymerization of High Performance PEDOT Counter Electrodes for Pt-Free Dye-Sensitized Solar Cells. *Electrochim. Acta* **2012**, *83*, 221−226.

(8) Trevisan, R.; Döbbelin, M.; Boix, P. P.; Barea, E. M.; Tena-Zaera, R.; Mora-Seró, I.; Bisquert, J. PEDOT Nanotube Arrays as High Performing Counter Electrodes for Dye Sensitized Solar Cells. Study of the Interactions Among Electrolytes and Counter Electrodes. *Adv. Energy Mater.* **2011**, *1*, 781−784.

(9) Allen, M. J.; Tung, V. C.; Kaner, R. B. Honeycomb Carbon: A Review of Graphene. *Chem. Rev.* **2009**, *110*, 132−145.

(10) Huang, X.; Qi, X.; Boey, F.; Zhang, H. Graphene-Based Composites. *Chem. Soc. Rev.* **2012**, *41*, 666−686.

(11) Kim, S. R.; Parvez, M. K.; Chhowalla, M. UV-Reduction of Graphene Oxide and Its Application as an Interfacial Layer to Reduce the Back-Transport Reactions in Dye-Sensitized Solar Cells. *Chem. Phys. Lett.* **2009**, *483*, 124−127.

(12) Wang, G.; Xing, W.; Zhuo, S. The Production of Polyaniline/Graphene Hybrids for Use as a Counter Electrode in Dye-Sensitized Solar Cells. *Electrochim. Acta* **2012**, *66*, 151−157.

(13) Sun, Y.; Wilson, S. R.; Schuster, D. I. High Dissolution and Strong Light Emission of Carbon Nanotubes in Aromatic Amine Solvents. *J. Am. Chem. Soc.* **2001**, *123*, 5348−5349.

(14) Qian, Z. S.; Wang, C.; Feng, H.; Chen, C. C.; Zhou, J.; Chen, J. R. Well Dispersed Single-Walled Carbon Nanotubes with Strong Visible Fluorescence in Water for Metal Ions Sensing. *Chem. Commun.* **2011**, *47*, 7167−7169.

(15) Tang, Q.; Wu, J.; Sun, X.; Li, Q.; Lin, J. Shape and Size Control of Oriented Polyaniline Microstructure by a Self-Assembly Method. *Langmuir* **2009**, *25*, 5253−5257.

(16) Yang, C.; Wang, X.; Du, P. C.; Liu, P. Polyaniline/Carbon Nanotube Multi-Layered Hollow Microspheres with Sandwich Structure and Their Electrochemical Performance. *Synth. Met.* **2013**, *179*, 34−41.

(17) Wu, T. M.; Lin, Y. W.; Liao, C. S. Preparation and Characterization of Polyaniline/Multi-Walled Carbon Nanotube Composites. *Carbon* **2005**, *43*, 734−740.

(18) Bavio, M. A.; Acosta, G. G.; Kessler, T. Synthesis and Characterization of Polyaniline and Polyaniline-Carbon Nanotubes Nanostructures for Electrochemical Supercapacitors. *J. Power Sources* **2014**, *245*, 475−481.

(19) Bahceci, S.; Toppare, L.; Yurtsever, E. Hydrogen Bonding in Polyanilines. *Synth. Met.* **1994**, *68*, 57−60.

(20) Minto, C. D. G.; Vaughan, A. S. Orientation and Conductivity in Polyaniline: 1. *Polymer* **1997**, *38*, 2683−2688.

(21) Hunter, C. A. The Role of Aromatic Interactions in Molecular Recognition. *Chem. Soc. Rev.* **1994**, *23*, 101−109.

(22) Wu, J.; Tang, Q.; Li, Q. Self-Assembly Growth of Oriented Polyaniline Arrays: A Morphology and Structure Study. *Polymer* **2008**, *49*, 5262−5267.

(23) Tang, Q.; Wu, J.; Sun, X.; Li, Q.; Lin, J.; Fan, L. Polyacrylamide-Controlled Growth of Centimeter-Scaled Polyaniline Fibers. *Polymer* **2009**, *50*, 752−755.

(24) Baibarac, M.; Baltog, I.; Godon, C.; Lefrant, S.; Chauvet, O. Covalent Functionalization of Single-Walled Carbon Nanotubes by Aniline Electrochemical Polymerization. *Carbon* **2004**, *42*, 3143−3152.

(25) Cochet, M.; Maser, W. K.; Benito, A. M.; Callejas, M. A.; Martinez, M. T.; Benoit, J. M.; Schreiber, J.; Chauvet, O. Synthesis of a New Polyaniline/Nanotube Composite: "In-Situ" Polymerisation and Charge Transfer Through Site-Selective Interaction. *Chem. Commun.* **2001**, 1450−1451.

(26) Saito, Y.; Kubo, W.; Kitamura, T.; Wada, Y.; Yanagida, S. I^-/I_3^- Redox Reaction Behavior on Poly(3,4-Ethylenedioxythiophene) Counter Electrode in Dye-Sensitized Solar Cells. *J. Photochem. Photobiol., A* **2004**, *164*, 153−157.

(27) Zeng, W.; Fang, G.; Wang, X.; Zheng, Q.; Li, B.; Huang, H.; Tao, H.; Liu, N.; Xie, W.; Zhao, X. Z.; Zou, D. Hierarchical Porous Nano-Carbon Composite: Effective Fabrication and Application in Dye Sensitized Solar Cells. *J. Power Sources* **2013**, *229*, 102−111.

(28) Wu, M.; Lin, X.; Wang, Y.; Wang, L.; Guo, W.; Qi, D.; Peng, X.; Hagfeldt, A.; Grätzel, M. Economical Pt-Free Catalysts for Counter Electrodes of Dye-Sensitized Solar Cells. *J. Am. Chem. Soc.* **2012**, *134*, 3419−3428.

(29) Wang, M. K.; Anghel, A. M.; Marsan, B.; Ha, N. L. C.; Pootrakulchote, N.; Zakeeruddin, S. M.; Grätzel, M. CoS Supersedes Pt as Efficient Electrocatalyst for Triiodide Reduction in Dye-Sensitized Solar Cells. *J. Am. Chem. Soc.* **2009**, *131*, 15976−15977.